

# Improving the Behaviour of Vision Transformers with Token-consistent Stochastic Layers

Nikola Popovic<sup>1</sup>, Danda Pani Paudel<sup>1</sup>, Thomas Probst<sup>1</sup>, Luc Van Gool<sup>1,2</sup>

<sup>1</sup> Computer Vision Laboratory, ETH Zurich, Switzerland

<sup>2</sup> VISICS, ESAT/PSI, KU Leuven, Belgium

{nipopovic, paudel, probstt, vangool}@vision.ee.ethz.ch

**Abstract.** We introduce token-consistent stochastic layers in vision transformers, without causing any severe drop in performance. The added stochasticity improves network calibration, robustness and strengthens privacy. We use linear layers with token-consistent stochastic parameters inside the multilayer perceptron blocks, without altering the architecture of the transformer. The stochastic parameters are sampled from the uniform distribution, both during training and inference. The applied linear operations preserve the topological structure, formed by the set of tokens passing through the shared multilayer perceptron. This operation encourages the learning of the recognition task to rely on the topological structures of the tokens, instead of their values, which in turn offers the desired robustness and privacy of the visual features. The effectiveness of the token-consistent stochasticity is demonstrated on three different applications, namely, network calibration, adversarial robustness, and feature privacy, by boosting the performance of the respective established baselines.

## 1 Introduction

Deep neural networks have shown to benefit from some level of stochasticity in various forms including regularization [89], optimization [87,40,86], data augmentation [16], as well as monte-carlo sampling for variational inference [48,26,84,103] or uncertainty estimation [26,27,45]. In general, it is however not clear how much and what form of stochasticity is desired for given neural architectures and for the tasks to be performed.

In this work, we introduce and systematically analyze the effect of token-consistent stochastic layers in vision transformers (ViTs) [20]. ViTs are networks of gripping interest, not only due to their widespread use but also due to their versatility. In turn, transformer architectures allow us to introduce stochastic layers in a controlled and tractable manner. This is achieved by performing token-consistent stochastic operations inside each block of the transformer, without altering the architecture or introducing additional learnable parameters. It is only necessary to briefly fine-tune the ViT, in order to adapt it to the stochasticity. These stochastic layers are introduced in an attempt to render the visual features more robust, private and suitable for good calibration, while maintaining the recognition performance of the initial visual transformers.

One important aspect of our way of injecting stochasticity is with regard to its consistency across the tokens. More precisely, we perform the stochastic linear operation with the same sample on all token features passing through a given multilayer perceptron (MLP), with a completely non-informative uniform distribution as the stochasticity source. Such token-consistent linear operations preserve the topological structures, invariant under affine transformations. Therefore, our way of injecting stochasticity encourages recognition to rely on the topological structures formed by the tokens, instead of their values. We demonstrate the effectiveness of token-consistent stochastic layers through improvements on the calibration and robustness of the vision transformers. The improved behaviours are demonstrated by comparing against the existing methods and the established baselines. Furthermore, the visual features are more private, when shared, because it is more difficult to reconstruct the input image due to the preformed stochastic operations. In this process, the privacy is achieved without severe impacts on image recognition. Our process of stochasticity injection tailored to vision transformers differs from existing ones [89,84,72,103] in one or more of these aspects: computational, tractability, or performance. The details are discussed in Section 3, 4 and 5.

The key contributions of this work are:

- We propose a token-consistent stochastic layer, which can be inserted in standard vision transformers without modifying the original architecture.
- We study the behaviour of the proposed stochasticity through exhaustive experiments on the ImageNet [80] benchmark dataset.
- We demonstrate its effectiveness on network calibration, adversarial robustness, and feature privacy, without severe impacts on image recognition.

## 2 Related Work

**Vision Transformer.** The transformer was first introduced in natural language processing [94,18,19,101], based on the self-attention mechanism [94]. In order to capture context across input sequences, the transformer employs multi-head self-attention and multi-layer perceptron modules, allowing for global interaction. Through the seminal work of ViT [20], transformers have successfully entered the vision domain. Vision transformers achieve state-of-the-art performance on problems including image classification [60,104,97], object detection [10], semantic/instance segmentation [108], and video segmentation [98]. For a more complete survey of vision transformers, we refer to [46].

**Stochasticity in Neural Networks.** Stochasticity has been a subject of study with regards to its effects on regularization and optimization [89,68,86], data augmentation [16,59], monte-carlo sampling for variational inference of latent variables [48] and model parameters [26,47], as well as generative modelling [48,66,43]. Furthermore, noise injection has been successfully applied to uncertainty estimation and network calibration [26,27,45,56] and adversarial robustness [1,77,14], and network compression [17].

**Confidence calibration.** In real-world decision making systems, classification networks should also indicate when they are likely to be incorrect [67,32]. While it was shown early on that shallow neural networks typically produce well-calibrated probabilities [69], it was discovered later that modern networks are not well-calibrated [32]. MC-Dropout [27,89] and Deep Ensembles [55] are the most popular techniques for combating this issue. A more structured way to drop model parameters is also presented as a good solution [21]. A thorough analysis of the calibration level of vision transformer architectures can be found at [65].

**Adversarial robustness.** A small adversarial perturbation in pixel intensities can lead to a severe drop in performance of accurate deep networks [90,29]. Most of the popular adversary attacks exploit the networks differentiability [90,29,62,3,53,64]. Numerous approaches were proposed to defend against these attacks, which we roughly categorize into adversarial training [54,83,99,62,106], certified defenses [14,15,105,82], gradient regularization [13,78,25,71,41,31], and stochasticity injection [77,9,74,57]. Furthermore, it is interesting that adversarially robust networks have other beneficial properties [81,38,44].

**Feature privacy.** Sharing image features is an important part of collaborative distributed systems [85,79,58]. Applications include camera localization [88], structure-from-motion [28], federated learning [7,42,49], or split learning/inference [33,95]. To address privacy issues, [75] obfuscates the geometry, homomorphic encryption guarantees privacy of feature extraction [76,36], retrieval [22], and federated learning [23]. However, these methods do not readily extend to many practical cases of distributed learning, like split learning [33,95]. Even though the feature extraction removes information from the input image, it is still possible reconstruct the input [93,107,102,96] or private attributes [5,85].

### 3 Background

The goal of introducing stochasticity by noise injection is to teach a network to (not) focus on specific aspects of the data. We now present our hypothesis that the injection of noise into a transformer architecture, under certain conditions, guides the network to rely on topological features.

**General Topology:** Given a set of  $n$  points,  $\mathcal{X} = \{\mathbf{x}_i\}_{i=1}^n \in \mathbb{R}^d$  assumed to be sampled on or near some underlying topological space  $X \subseteq \mathbb{R}^d$ , we are interested in the information about the topology of  $X$ . To be precise, we are interested to perform a stochastic modification of the point set  $\mathcal{X}$  such that the underlying topology of  $X$  remains unchanged in some sense. Informally two topological spaces  $X$  and  $Y$  are equivalent ( $X \cong Y$ ) if there is a continuous function  $f : X \rightarrow Y$  that has an inverse  $f^{-1}$  which is also continuous. Whenever the mapping  $f$  is feasible, we call these two topological spaces  $X$  and  $Y$  homeomorphic and  $f$  is their homeomorphism. For a more detailed and formal account on topology please refer to [34,11].

In this work, the set of points  $\mathcal{X}$  are the features generated by  $n$  tokens of the transformers. We wish to encourage the recognition task to rely upon the topology of  $X$ , instead of the entries of the feature vectors. *Therefore, we would*

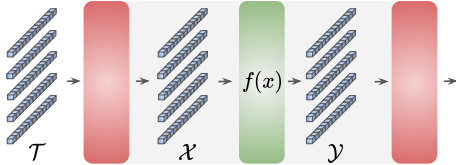


Fig. 1. A single stochastic multilayer perceptron with multiple input tokens  $\mathcal{T}$ . At the intermediate stage, the stochastic layer  $f(\mathbf{x})$  homeomorphically maps features  $\mathcal{X}$  to  $\mathcal{Y}$ .

*like to preserve the topology of  $X$  during the stochastic operations.* To do so, we perform a stochastically homeomorphic mapping of the point set  $\mathcal{X}$ . In our experiments, we use an invertible linear transformation –around the identity map for numerical stability– to represent  $f$ , which is by design a homeomorphic mapping. A graphical illustration of the performed operations is shown in Figure 1.

**Inside the multilayer perceptron in ViTs:** ViTs divide images into multiple tokens. These tokens are processed by attention modules followed by multilayer perceptrons (MLPs). We are interested in introducing stochasticity within the processing pipeline of the MLPs. Let us consider, without lack of generality, that the intermediate features inside an MLP for tokens  $\mathcal{T} = \{t_i\}_{i=1}^n$  are given by  $\mathcal{X} = \{\mathbf{x}_i\}_{i=1}^n \in \mathbb{R}^d$ . A homeomorphic mapping  $f: X \rightarrow Y$ , in a fully stochastic fashion, is applied to the set of features  $\mathcal{X}$  resulting into the mapped set  $\mathcal{Y}$ . We continue processing the mapped features  $\mathcal{Y}$  similar to  $\mathcal{X}$ , as if the stochastic layer represented by  $f$  was absent. We represent  $f$  as a square diagonal matrix  $\mathbf{A} \in \mathbb{R}^{d \times d}$  with non-zero diagonal entries. Then the operation by the introduced stochastic layer in the form,  $\mathbf{y}_i = f(\mathbf{A}, \mathbf{x}_i) = \mathbf{A}\mathbf{x}_i, \forall \mathbf{x}_i \in \mathcal{X}$ , ensures  $f: X \rightarrow Y$  to be homeomorphic. Please note that the mappings by square diagonal matrices with non-zero entries are continuous with their inverse being continuous as well. Other choices of  $f$  could be made as well, but we study the behaviour of ViTs with a relatively simple function  $f$ .

## 4 Token-consistent Stochastic Layers in Vision Transformers

Let the input image be denoted as  $\mathcal{I} \in \mathbb{R}^{H \times W \times 3}$ , where  $H$  is the height and  $W$  is the width of the image. The image is represented using 3 color channels. A feature extractor  $F$  takes the image  $\mathcal{I}$  as the input and produces a feature map  $\mathcal{F} = F(\mathcal{I})$ . Usually  $\mathcal{F} \in \mathbb{R}^{\frac{H}{s} \times \frac{W}{s} \times C}$ , meaning that its spatial dimensions are downscaled by a factor of  $s$  compared to the image  $\mathcal{I}$  and that it has  $C$  channels. The feature map  $\mathcal{F}$  can be used for various tasks. As one option, the feature map can be an input to a classification model  $C$  to produce  $\mathcal{O} = C(\mathcal{F}) = C(F(\mathcal{I}))$ , where  $\mathcal{O} \in \mathbb{R}^m$  and  $m$  is the number of classes. It can also be given to a regression model  $R$  to produce  $\mathcal{O} = R(\mathcal{F})$ , where  $\mathcal{O} \in \mathbb{R}^m$  and  $m$  is the number of regressed values. Another option is to give it to a model  $D$  to produce an image-to-image translation output  $\mathcal{O} = D(\mathcal{F})$ , where  $\mathcal{O} \in \mathbb{R}^{H \times W \times m}$ . This can be used for various tasks like semantic segmentation, depth estimation, flow estimation, etc.

Generally speaking, a Vision Transformer (ViT) [20] is one type of feature extractor  $F$ . First, it takes the input image  $\mathcal{I}$  and divides it spatially into  $k \times k$  patches to obtain  $\tilde{\mathcal{I}} \in \mathbb{R}^{\frac{H}{k} \times \frac{W}{k} \times 3k^2}$ , which represents  $n_T = \frac{H}{k} \frac{W}{k}$  token vectors of dimension  $3k^2$ . A popular choice is  $k = 16$  [20,92]. Then, each token vector is embedded into  $d_T$  dimensions, using the same affine transformation, to obtain  $\mathcal{F}_0 \in \mathbb{R}^{n_T \times d_T}$ . Optionally, a classification or regression token can be appended to  $\mathcal{F}_0$ , which would result in  $\hat{n}_T = \frac{H}{k} \frac{W}{k} + 1$ . This token is used to make a prediction for the final task. Next, a positional encoding  $\mathcal{P} \in \mathbb{R}^{n_T \times d_T}$  is added to  $\mathcal{F}_0$  which gives  $\tilde{\mathcal{F}}_0 = \mathcal{F}_0 + \mathcal{P}$ . The purpose of the positional encoding  $\mathcal{P}$  is to add information about which token in  $\mathcal{F}_0$  corresponds to which spatial location of the input image  $\mathcal{I}$ . The transformer then uses  $l$  consecutive transformer blocks  $B_i$  to extract features. Each block  $B_i$  takes the output of the previous block  $\mathcal{F}_{i-1}$  as its input and produces  $\mathcal{F}_i = B_i(\mathcal{F}_{i-1})$ , where  $\mathcal{F}_i \in \mathbb{R}^{n_T \times d_T}$ . The first block takes  $\tilde{\mathcal{F}}_0$  as input. To obtain the final feature map  $\mathcal{F}$ , we usually take the output of the last block  $\mathcal{F}_l$ , discard the optional classification or regression token, and spatially rearrange it back as  $\mathcal{F} \in \mathbb{R}^{\frac{H}{s} \times \frac{W}{s} \times C}$ , where  $C = d$  and  $s = k$ .

Each transformer block  $B_i$  is composed of a Multi-head Self Attention block (MSA), followed by a Multilayer Perceptron (MLP) [94,20]. Self-attention is a spatially global operation, where every token interacts with every other token and thus information is shared across spatial dimensions. Multiple heads in the MSA block are used for more efficient computation and for extracting more diverse features. The MSA block executes the following operations:

$$\mathcal{Z}_i = \text{MSA}(\text{LN}(\mathcal{F}_{i-1})) + \mathcal{F}_{i-1}, \quad (1)$$

where LN represents layer normalization [4]. The MSA block is followed by the MLP block, which processes each token separately using the same multilayer perceptron. This block processes the tokens, after their spatially global interactions in the MSA block, by sharing and refining the representations of each token across all of its channels. The MLP block executes the following operations:

$$\mathcal{F}_i = \text{MLP}(\text{LN}(\mathcal{Z}_i)) + \mathcal{Z}_i, \quad \mathcal{Z}_i \in \mathbb{R}^{n_T \times d_T}. \quad (2)$$

In the following, we omit the block index  $i$  for simplicity, and unpack (2):

$$\mathcal{Z}^{LN} = \text{LN}(\mathcal{Z}), \quad \mathcal{Z}^{LN} \in \mathbb{R}^{n_T \times d_T}, \quad (3)$$

$$\mathcal{Z}^{FC_1} = \text{FC}(\mathcal{Z}^{LN}), \quad \mathcal{Z}^{FC_1} \in \mathbb{R}^{n_T \times d}, \quad (4)$$

$$\mathcal{Z}^{act} = \sigma(\mathcal{Z}^{FC_1}), \quad \mathcal{Z}^{act} \in \mathbb{R}^{n_T \times d}, \quad (5)$$

$$\mathcal{Z}^{FC_2} = \text{FC}(\mathcal{Z}^{act}), \quad \mathcal{Z}^{FC_2} \in \mathbb{R}^{n_T \times d_T}, \quad (6)$$

$$\mathcal{F} = \mathcal{Z}^{FC_2} + \mathcal{Z}, \quad \mathcal{F} \in \mathbb{R}^{n_T \times d_T}, \quad (7)$$

where FC is the fully connected layer and  $\sigma$  the activation function.

We inject noise into the transformer, by injecting noise into the intermediate feature map  $\mathcal{Z}^{FC_1} \in \mathbb{R}^{n_T \times d}$  of every MLP. More specifically, this is achieved by multiplying all of its tokens  $\mathbf{z}^{FC_1}$  with a stochastic square diagonal matrix

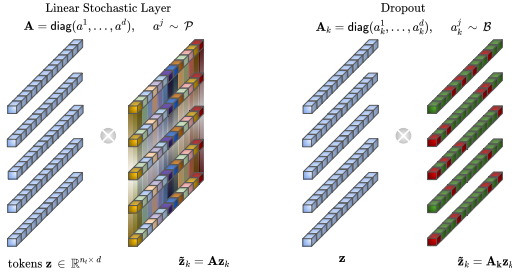


Fig. 2. Token-consistent Stochastic Layer compared to dropout [89] regularization, illustrated with the help of vision transformer’s tokens.

$\mathbf{A} \in \mathbb{R}^{d \times d}$  to obtain  $\tilde{\mathbf{z}}^{FC_1} \in \mathbb{R}^d$ , and thus  $\tilde{\mathbf{Z}}^{FC_1} \in \mathbb{R}^{n_T \times d}$  as,

$$\begin{aligned} \tilde{\mathbf{z}}_k^{FC_1} &= \mathbf{A} \mathbf{z}_k^{FC_1}, \quad k = 1 \dots n_T \\ \mathbf{A} &= \text{diag}(a^1, a^2, \dots, a^d), \quad a^j \sim \mathcal{P}. \end{aligned} \quad (8)$$

This corresponds to multiplying the channel dimension  $j$  of all tokens with the same  $a^j$  (token-consistent). The elements of  $\mathbf{A}$  are sampled from a continuous random distribution  $\mathcal{P}$ , independently for each block  $\mathbf{B}_i$ . The matrix  $\mathbf{A}$  is sampled only once per input in  $\mathbf{B}_i$ , meaning that each token’s feature vector  $\tilde{\mathbf{z}}^{FC_1}$  gets multiplied element-wise with the same noise vector, akin to a stochastic linear layer. The feature map  $\tilde{\mathbf{Z}}^{FC_1}$  is used instead of  $\mathbf{Z}^{FC_1}$  in (5). We choose to inject the noise to the feature map  $\mathbf{Z}^{FC_1}$ , because it has the highest dimensionality in the block ( $d > d_T$ ), thus the impact of the noise will be the highest. If  $\mathbf{A}_k$  was re-sampled for different tokens  $k$ , and  $\mathcal{P}$  was the Bernoulli distribution, this would correspond to the commonly known dropout regularization [89]. Figure 2 highlights the difference between our method and dropout visually.

## 5 Experiments

We now empirically study the effectiveness of token-consistent stochastic layers, by gauging their impact on confidence calibration and robustness of the vision transformers, under different strength of stochasticity. At the same time, we analyse the trade-offs with respect to classification accuracy, privacy and transferability of the visual features. For each of these aspects, we compare our method to established baselines and applicable state-of-the-art alternatives, in order to demonstrate its impact in a holistic manner. For additional results, more detailed discussions and a further analysis with regards to topological properties, we would like to refer to our supplementary materials.

We choose the DeiT-S architecture [92] as our main representative of vision transformers in our experiments. DeiT-S is one specific instance of the ViT [20] and has a parameter count and computational complexity similar to ResNet-50 [35]. When analysing the effect of our stochastic layers on the ImageNet

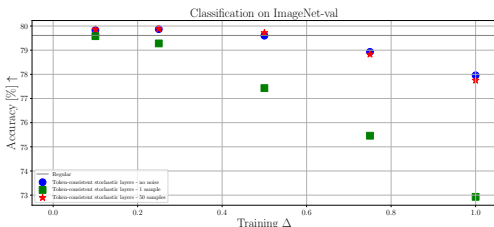


Fig. 3. **ImageNet classification.** Token-consistent stochastic layers bring no significant drop in accuracy, even with strong levels of noise. Performance is better when  $a^j$  is fixed to the mean, or when using Monte Carlo sampling during inference.

accuracy in Section 5.1, we also verify that the behaviour is consistent across vision transformer architectures. After asserting a tenable decrease in accuracy, we continue to evaluate the suitability of the proposed stochastic layers with regards to confidence calibration in Section 5.2, and defending adversarial attacks Section 5.3. To round up the empirical analysis, we further investigate the impact visual features with regards to privacy in collaborative settings, and their ability to generalize to new tasks in Sections 5.4 and 5.5, respectively.

## 5.1 Effects on ImageNet Accuracy

**Training procedure.** To explore the general behaviour of our method we use the ILSVRC-2012 ImageNet-1k dataset, which contains 1.2M training and 50000 validation images grouped into 1000 classes [80]. The DeiT-S model pre-trained on ImageNet-1k is used as a starting point for all experiments in Section 5, unless otherwise mentioned. All the details regarding the pre-training procedure are contained in [92]. We insert the token-consistent stochastic layer from (8) into every block of the DeiT-S and fine-tune it for 30 epochs. We choose  $\mathcal{P}$  to be uniform,  $\mathcal{P} \sim \mathcal{U}(1 - \Delta, 1 + \Delta)$ , since it is a completely non-informative distribution and thus the strongest source of noise. During this fine-tuning process, we use the AdamW optimizer [61] and a cosine scheduler with a learning rate of  $10^{-5}$ , which gradually decays to  $10^{-6}$ . We also turn off DropPath [37] and use the ReLU activation in order to introduce the noise to a deterministic baseline with a (piecewise) linear impact. All other settings remain as in pre-training.

**Experiments.** We analyzing the predictive performance of stochastic layers on the ImageNet validation set, measured through classification accuracy. As presented in Figure 3, there is no significant drop in accuracy, even when using high noise levels during inference. The network performs better when  $a^j$  from (8) is set as the mean of the training noise distribution  $\mathbb{E}[\mathcal{P}]$  during inference (noise turned off). Also, the network preforms better when multiple predictions are sampled ( $a^j \sim \mathcal{P}$  independently sampled for each block and prediction) and averaged in a Monte Carlo fashion. However, the inference also works reasonably well when we just sample once. This is surprising given the fact that  $a^j$ , which

Table 1. **ImageNet classification.** Performance of token-consistent stochastic layers.

(a) Using the same sample of  $\mathbf{A}$  from (8) for different tokens (token-consistent) is a stronger form of noise compared to sampling different  $\mathbf{A}$  for different tokens.

		Accuracy $\uparrow$		
		Noise off	$N = 1$	$N = 50$
DeiT-S		79.61%		
$\Delta = 0.5$	DeiT-S + dropout [89]	79.60%	78.54%	79.79%
	DeiT-S + not-token-consistent uniform	79.63%	78.59%	79.81%
	DeiT-S + token-consistent uniform	79.60%	77.43%	79.72%
$\Delta = 1.0$	DeiT-S + dropout [89]	77.93%	76.18%	78.74%
	DeiT-S + not-token-consistent uniform	77.99%	75.85%	78.63%
	DeiT-S + token-consistent uniform	77.96%	72.93%	77.75%

(b) Token-consistent stochastic layers also behave well on different architectures.

		Accuracy $\uparrow$		
		Noise off	$N = 1$	$N = 50$
DeiT-S [92]	no noise	79.61%		
	+ $\Delta = 0.1$	79.83%	79.58%	79.86%
	+ $\Delta = 0.5$	79.60%	77.43%	79.72%
	+ $\Delta = 1.0$	77.96%	72.93%	77.75%
Swin-T [60]	no noise	81.03%		
	+ $\Delta = 0.1$	81.02%	81.02%	81.09%
	+ $\Delta = 0.5$	81.05%	79.40%	81.07%
	+ $\Delta = 1.0$	80.20%	75.95%	80.08%

(c) The networks with token-consistent stochastic layers are also successfully trained from scratch on 100 randomly chosen classes of the ImageNet-1k dataset.

		Accuracy $\uparrow$		
		Noise off	$N = 1$	$N = 50$
DeiT-S		89.18%	89.18%	89.18%
DeiT-S + $\Delta = 0.1$		89.40%	89.30%	89.28%
DeiT-S + $\Delta = 0.5$		89.48%	88.58%	89.48%
DeiT-S + $\Delta = 1.0$		89.06%	88.00%	89.24%

multiplies token channels, is sampled from a completely non-informative uniform distribution. In Table 1a, we see that our stochastic layer preforms slightly worse than regular dropout, indicating that it is a stronger source of stochasticity. When analyzing a certain  $\Delta$ , we chose the dropout probability such that it has the same mean and variance. Also, when the noise matrix  $\mathbf{A}$  is sampled independently for each token (non-token-consistent), the performance is slightly better compared to being token-consistent (same  $\mathbf{A}$  sample for every token). This is surprising as one would expect having more independent noise elements in the stochastic layer would produce a stronger noise effect. The choice of noise strength and inference mode will depend on the final use-case. In the following subsections, we analyse the involved trade-offs to guide this decision.

Next, we insert the stochastic layers into the state-of-the-art Swin transformers [60] to verify that the proposed method is not tailored for a specific ViT architecture. More precisely, we fine tune the Swin-T model, which has a parameter count and computational complexity similar to DeiT-S, following the



same fine-tuning procedure as previously described. From Table 1b, we observe that our stochastic layers behave well across different transformer architectures.

The aim of this paper is to show the benefits of integrating proposed stochastic layers into vision transformers, with just fine-tuning and without architectural modifications. Nevertheless, we want to make sure that the training convergence is not just because of very good initial weights. Therefore, we conduct an experiment where we train from scratch on a 100 randomly chosen classes of the ImageNet-1k dataset. The models are trained followings the settings from [92]. In Table 1c, we see that there is no problem learning with our stochastic layers.

## 5.2 Effects on Confidence Calibration

**Problem Definition.** In practice, any inference algorithm is only useful for a decision-making system, if it can also give an indication about the confidence of its predictions. Intuitively, if a well-calibrated classifier outputs a prediction with a confidence of  $p$  (e.g. softmax score), we expect the classifier to be correct with probability  $p$ . In the context of supervised multi-class classification, random variables  $X \in \mathcal{X}$  and  $Y \in \mathcal{Y}$  represent the input and labels respectively. Then a classifier  $h(X) = (\hat{Y}, \hat{P})$ , predicting a label  $\hat{Y}$  and an associated confidence  $\hat{P}$ , would be perfectly calibrated if  $\mathbb{P}(\hat{Y} = Y | \hat{P} = p) = p \quad \forall p \in [0, 1]$ . In particular, we are interested in quantifying the quality of calibration. To this end, we analyse the expected calibration error (ECE),  $\mathbb{E}_{\hat{P}} \left[ \mathbb{P}(\hat{Y} = Y | \hat{P} = p) - p \right]$ . It measures the expected disparity between prediction confidence and accuracy, and would be 0 in the case of perfect calibration. To estimate this value using finite samples, [67] sorts network predictions  $\hat{P}$  into  $M$  equidistant bins. Then the ECE is approximated by computing the disparity between accuracy and confidence for samples from each bin as,  $\text{ECE} = \sum_{m=1}^M \frac{|B_m|}{n} |\text{acc}(B_m) - \text{conf}(B_m)|$ , where  $B_m$  denotes the indices of all samples in the interval  $(\frac{m-1}{M}, \frac{m}{M}]$ ,  $\text{acc}(B_m) = \frac{1}{|B_m|} \sum_{i \in B_m} \mathbf{1}(\hat{y}_i = y_i)$  calculates the accuracy on that interval and  $\text{conf}(B_m) = \frac{1}{|B_m|} \sum_{i \in B_m} \hat{p}_i$  calculates the confidence on that interval. For our experiments, we compare the ECE with  $M = 15$  bins [32] on the ImageNet-1k validation set.

**Experiments.** We evaluate the calibration of vision transformers, trained with the procedure described in Section 5.1, by comparing the ECE metric of token-consistent stochastic layers to the respected baselines. One very effective method for improving network calibration is the temperature scaling, where the optimal softmax temperature is usually chosen on the validation set [32]. This method can be used on top of any classification model with a softmax output, and was recently shown to work well with transformers [65]. Monte Carlo dropout [27] is one of the most popular methods for improving calibration, therefore one baseline is placing dropout layers instead of token-consistent stochastic layers. To create a fair counterpart to our model with a noise level  $\Delta$ , we chose the dropout probability such that it has the same mean and variance. Recently proposed

Table 2. **Confidence calibration.** Token-consistent stochastic layers achieve better calibration compared to several respected baselines and non-token-consistent uniform noise. The calibration is better for stronger noise, and with Monte Carlo sampling.

		ECE↓ (Accuracy↑)		
DeiT-S		0.088(79.8%)		
DeiT-S + temp. [32]		0.026(79.8%)		
DeiT-S + masksembles [21] + temp. [32]		0.017(76.7%)		
DeiT-S + stochastic layers + temp. [32]		Noise off	$N = 1$	$N = 50$
$\Delta = 0.5$	dropout [27]	0.022(79.6%)	0.020(78.7%)	0.019(79.7%)
	not-token-consistent uniform	0.023(79.6%)	0.022(78.6%)	0.019(79.8%)
	token-consistent uniform	0.023(79.6%)	0.020(77.5%)	0.017(79.6%)
$\Delta = 1.0$	dropout [27]	0.019(77.9%)	0.019(76.1%)	0.014(78.7%)
	not-token-consistent uniform	0.019(80.0%)	0.016(76.0%)	0.014(78.6%)
	token-consistent uniform	0.016(78.0%)	0.012(73.1%)	<b>0.010(77.6%)</b>

masksembles [21] are the SotA method for improving calibration in CNNs, so another baseline is placing masksemble layers instead of token-consistent stochastic layers. Finally, one more baseline is the non-token-consistent stochastic layers, where the noise matrix  $\mathbf{A}$  from (8) is sampled differently for different tokens.

The results of the experiments are summarized in Table 2. We observe that using temperature scaling in any setup improves the calibration. Also, we see that our token-consistent stochastic layers bring better calibration than other baselines, without severe impacts on image recognition. This effect is stronger as the strength of the noise increases, as well as when using Monte Carlo sampling.

### 5.3 Effects on Adversarial Robustness

**Problem definition.** Besides accuracy and calibration, another important aspect of the network is its behaviour with respect to adversarial examples [90,29]. In general, adversarial attacks exploit the differentiability of the network  $f(x)$  and its prediction loss  $\mathcal{L}(f(x), l)$ , with respect to the input image  $x$ , where  $l$  is the label. Given the true label  $l_t$ , the attack aims to slightly modify the input  $x$  to maximize the prediction loss for label  $l_t$ . To craft stronger adversarial samples, the fast gradient sign method (FGSM) [29] is repeated multiple times with step size  $\alpha$ , followed by a projection to an  $\epsilon$  hypercube around the initial sample  $x$ ,  $\hat{x}^k = \Pi_\epsilon [x^{k-1} + \alpha \text{sgn}(\nabla_x \mathcal{L}(f(\hat{x}^{k-1}), l))]$ . This is known as the projected gradient descent (PGD) attack [62].

**Evaluation protocol.** In order to evaluate adversarial robustness, we craft adversarial examples for each image in the ImageNet-1k validation set, and test the model’s accuracy on them. We do this by using the PGD attack with 10 iterations (PGD-10). When crafting each adversarial example, we initialize the attack’s starting point randomly inside the  $\epsilon$ -hypercube. We restart this procedure 5 times to find the strongest attack and test for two different  $\epsilon$  constraints  $\epsilon = \{\frac{2}{255}, \frac{4}{255}\}$ , following the standard benchmark of [99,83]. The attack step size  $\alpha$  is 1 in both cases. When dealing with noise inside the network, the

Table 3. **Adversarial robustness.** In Table 3a, we see that our stochastic layers are more robust compared to the evaluated baselines. Table 3b shows that using Monte Carlo sampling with our stochastic layers improves adversarial robustness and clean accuracy, under adversarial training. This effect is stronger with stronger noise.

(a) Overview of the adversarial robustness compared to different baselines.

	Accuracy $\uparrow$			
	Adversarial training with $\epsilon = \frac{2}{255}$		Adversarial training with $\epsilon = \frac{4}{255}$	
	Clean samples	PDG-10 attack	Clean samples	PDG-10 attack
	DeiT-S	<b>79.61%</b>	0.43%	79.61%
DeiT-S + ours	77.75%	12.36%	77.75%	4.76%
DeiT-S + adv. tr. [99]	71.61%	42.33%	65.04%	27.24%
DeiT-S + PNI [77] + adv. tr. [99]	73.83%	45.16%	69.24%	31.18%
DeiT-S + ours + adv. tr. [99]	73.83%	<b>49.32%</b>	<b>70.47%</b>	<b>36.38%</b>

(b) Analysis of the effects of our stochastic layers on adversarial robustness.

		Accuracy $\uparrow$					
		Adversarial training with $\epsilon = \frac{2}{255}$ [99]			Adversarial training with $\epsilon = \frac{4}{255}$ [99]		
		Clean samples	PDG-10 attack	PDG-10 EoT attack	Clean samples	PDG-10 attack	PDG-10 EoT attack
		DeiT-S		71.61%	42.33%	42.33%	65.04%
DeiT-S + PNI [77] (layerwise)	$N = 1$	73.50%	44.84%	40.60%	68.77%	31.07%	25.90%
	$N = 50$	73.83%	45.16%	40.88%	69.24%	31.18%	26.02%
DeiT-S + PNI [77] (channelwise)	$N = 1$	72.88%	44.47%	40.96%	67.40%	30.22%	26.11%
	$N = 50$	73.47%	44.89%	41.37%	68.30%	30.37%	26.48%
DeiT-S + PNI [77] (elementwise)	$N = 1$	72.51%	44.49%	41.08%	67.02%	29.99%	26.13%
	$N = 50$	73.41%	44.85%	41.49%	68.01%	30.20%	26.54%
DeiT-S + ours ( $\Delta = 0.1$ )	$N = 1$	71.79%	42.90%	42.44%	65.23%	27.88%	27.39%
	$N = 50$	71.84%	42.91%	<b>42.53%</b>	65.29%	27.86%	<b>27.46%</b>
DeiT-S + ours ( $\Delta = 0.5$ )	$N = 1$	71.79%	44.51%	40.29%	66.53%	30.68%	25.80%
	$N = 50$	73.73%	46.21%	41.64%	68.65%	31.47%	26.58%
DeiT-S + ours ( $\Delta = 1.0$ )	$N = 1$	68.62%	45.37%	36.75%	65.40%	33.48%	23.30%
	$N = 50$	<b>73.83%</b>	<b>49.32%</b>	39.58%	<b>70.47%</b>	<b>36.38%</b>	24.92%
Iterations per attack		0	50	250	0	50	250

expectation-over-transformation (EoT) attack is usually more effective [2], since it exploits multiple noise samples to avoid gradient obfuscation and to find a common weakness. We also use it during evaluation with 5 expectation samples.

**Experiments.** Adversarial training is a very effective remedy for adversarial vulnerability [62], therefore we use it in our experiments. More specifically, we use the efficient adversarial training described in [99], which fits in our standard training protocol without much overhead. During this robust fine-tuning, regular hyperparameters remain the same as in Section 5.1, except for using 20 epochs now, because the optimization is more computationally demanding. Following [99], the step sizes during adversarial training are  $\alpha = \{\frac{2.5}{255}, \frac{5}{255}\}$  for  $\epsilon = \{\frac{2}{255}, \frac{4}{255}\}$ , respectively. One baseline is applying adversarial training during fine-tuning to the DeiT-S starting point described in Section 5.1. Furthermore, Parametric Noise Injection (PNI) [77] is a SotA adversarial defense when it

comes to stochasticity based defenses. Therefore, another baseline is replacing our stochastic layers for PNI layers in the vision transformer. In Table 3a we see that our token-consistent stochastic layers improves adversarial robustness beyond adversarial training. We also see that a better robustness is achieved compared to using the PNI baseline. Furthermore, introducing our stochastic layers brings small adversarial robustness, even without adversarial training.

Next, in Table 3b we see an analysis of the effects of token-consistent stochastic layers on robustness. The network is more robust with stronger noise and when networks are sampled in a Monte Carlo fashion. Also, the clean accuracy becomes higher with sampling. This is particularly interesting, since it has been shown that there is a trade-off between adversarial robustness and clean accuracy [106]. Moreover, under the EoT attack, our stochastic layers perform better than the SotA PNI [77]. Unfortunately though, neither method performs significantly better than the deterministic baseline. This may be attributed to the possibility of being able to estimate a reliable expectation of the gradients by means of Monte Carlo sampling. In fact, alternative methods could be designed to hinder the expectation estimation required for the EoT attack. More importantly, the EoT attack is significantly more computationally demanding than the PGD attack, making the attack itself more difficult to perform.

## 5.4 Effects on Privacy in Collaborative Settings

**Problem definition.** We consider a practical collaborative learning and inference setup  $\hat{y} = \Phi_2(\Phi_1(x)) = \Phi(x)$ , where  $\Phi_1$  is the client network executed on trusted devices and  $\Phi_2$  is a task network executed on an untrusted server using the clients’ activation  $z = \Phi_1(x)$  [85,79,58]. The client network  $\Phi_1$  is the first part of the network  $f$  which produces the feature map  $z = \tilde{Z}_i^{FC_1}$  from (8) of the  $i$ -th block. The client sends  $z$  to the server  $\Phi_2$ , which is the second part of the network  $\Phi$ . For collaborative inference, the server then predicts  $\hat{y} = \Phi_2(z)$ .

For collaborative learning, the client sends labelled  $(z, y)$  pairs to the server. In general, the server trains the network  $\Phi_2$ , and broadcasts the gradient to update  $\Phi_1$  [95]. We use a slightly different setting, where  $\Phi_1$  is a strong general feature extractor (e.g. pretrained on ImageNet), whose features allow for effective transfer to the desired tasks [50]. In this scenario, the  $\Phi_1$  does not update, while only  $\Phi_2$  is trained on the server using the data  $(z, y)$  from all participants.

Under our threat model, the untrusted server attempts to obtain sensitive information by recovering the input image  $x$  (e.g. a face or medical image). The input  $x$  is recovered from the client activation  $z = \tilde{Z}_i^{FC_1}$ , by using a reconstruction network  $\hat{x} = r(z)$ . The practical validity of this threat model is in the scenarios where a small number of training pairs  $(x, z)$  is obtained through a malicious or colluding client, who is participating in the collaborative setting [85]. Another scenario is when pairs  $(x, z)$  from a similar distribution are publicly available or intercepted. Therefore, it is very important for the shared feature map  $z$  to be private.

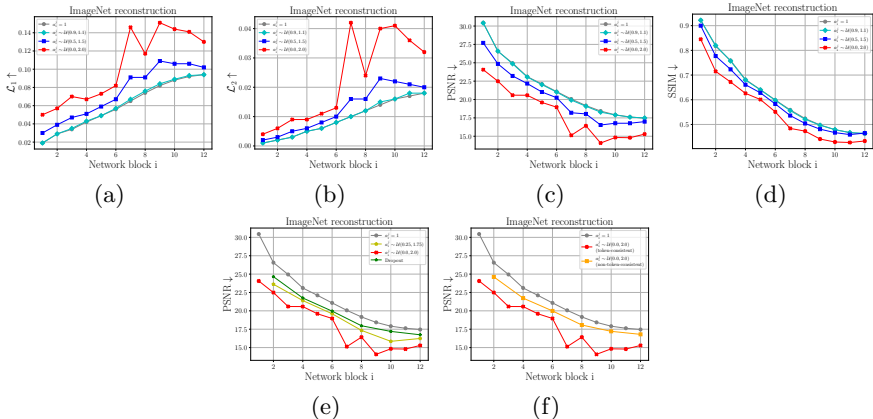


Fig. 4. **Privacy in collaborative inference.** In Figures 4a - 4d we see that stronger noise in our token-consistent stochastic layers makes the features more private. In Figures 4e we see that regular dropout preserves less privacy than our stochastic layers (dropout matches the variance of  $\mathcal{U}(0, 2)$  and has a similar classification accuracy as  $\mathcal{U}(0.25, 1.75)$ ). In Figure 4f we see that token-consistent noise is more private compared to the non-token-consistent version.

**Experiments.** In order to evaluate the privacy of shared features in the collaborative inference, we train a decoder to reconstruct the input image from the feature map  $z = \tilde{Z}_i^{FC_1}$ , from different blocks  $i$  of the models trained in Section 5.1. A good reconstruction quality indicates a weak protection of sensitive information, and thus low privacy. The decoder from [39] is used, after adjusting it to the spatial size of  $\tilde{Z}_i^{FC_1}$ . We use the  $L_1$  reconstruction loss to train the decoder on a small subset of ImageNet-1k, containing 20 randomly chosen classes. We evaluate the reconstruction quality by measuring the  $L_1$ ,  $L_2$ , peak signal to noise ratio (PSNR) and structural similarity index measure (SSIM) metrics. In Figures 4a - 4d we see that it is harder to reconstruct the input from feature maps  $\tilde{Z}_i^{FC_1}$  when using our stochastic layers. The gap to the deterministic network increases with stronger levels of noise. Next, in Figures 4e - 4f we see that our token-consistent stochastic layers preserve more privacy compared to regular dropout or the non-token-consistent version. These experimental results demonstrate the privacy benefits of our token-consistent stochastic layers for collaborative inference, on the basis of poor reconstruction quality. The additional comparisons with the related works in collaborative inference is beyond the scope of this paper, as they use tailored architectures, losses, and learning setups designed for the same [85, 79, 58].

In the case of collaborative learning, we train only  $\Phi_2$  on a new task of CIFAR10/100 [52] image classification. We model  $\Phi_2$  by two fully connected and one softmax layers, to address the task at hand. In Figure 5 we visualize the trade-off between the accuracy on the new tasks and the input reconstruction (feature privacy). We observe that using stochastic layers offers better privacy in

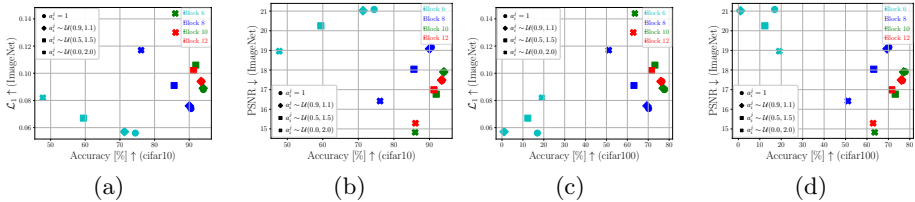


Fig. 5. **Privacy in collaborative learning.** Stochastic layers offer privacy and performance trade-offs whose operating point can be chosen in accordance to the use-case.

Table 4. **Transfer learning on 12 different tasks.** The token-consistent stochastic layers retain transferability across different noise levels.

		Aircraft [63]	Birdsnap [6]	CIFAR 10 [52]	CIFAR 100 [52]	Caltech 101 [24]	Caltech 256 [30]	Cars [51]	DTD [12]	Flowers [70]	Food [8]	Pets [73]	SUN 397 [100]
Pre- training	no noise	72.34%	70.41%	98.11%	87.41%	91.89%	83.85%	80.76%	73.46%	92.39%	87.06%	92.83%	62.34%
	$\Delta = 0.1$	72.52%	69.97%	98.36%	87.93%	91.55%	83.87%	82.13%	73.72%	94.02%	87.45%	93.10%	62.35%
	$\Delta = 0.5$	71.50%	69.58%	98.13%	87.65%	91.89%	84.07%	81.52%	73.94%	93.69%	87.10%	93.16%	62.79%
	$\Delta = 1.0$	72.40%	70.00%	98.29%	88.04%	91.85%	83.99%	81.99%	73.94%	93.61%	87.29%	93.08%	62.36%

this setting at a cost of task performance. With this knowledge one can choose a trade-off point, in accordance with the final task and the use-case.

## 5.5 Effects on Transfer Learning

To measure the impact of our stochastic layers on general image recognition performance, we compare the transferability of our features on a standard benchmark suite following the setup of [81]. We use the AdamW optimizer [61] with an initial learning rate of  $10^{-5}$  and weight decay of  $5 \times 10^{-2}$ . The transfer learning lasts for 150 epochs and the learning rate gets decayed by a factor of 10 every 50 epochs. Our findings are summarized in Table 4. Despite the tendency of big transformer architectures to quickly overfit, all compared method obtain competitive results. We observe that our token-consistent stochastic layers are able to retain their performance and sometimes even exceed the deterministic baseline. The transferability is retained across different noise levels.

## 6 Conclusion

In this work, we investigate the role of stochasticity in vision transformers. By interjecting token-consistent stochastic layers during both training and inference, we transform the feature activations of each multilayer perceptron, while preserving the topological structure of the activations. This transformation offers the robustness and privacy of visual features, while retaining the original predictive performance. We demonstrated the utility of our features for the applications of adversarial robustness, network calibration, feature privacy and transfer learning. From our experiments we conclude that our token-consistent stochastic layers are well behaved and our visual features offer exciting results on those tasks.

# Improving the Behaviour of Vision Transformers with Token-consistent Stochastic Layers

## Supplementary material

Nikola Popovic<sup>1</sup>, Danda Pani Paudel<sup>1</sup>, Thomas Probst<sup>1</sup>, Luc Van Gool<sup>1,2</sup>

<sup>1</sup> Computer Vision Laboratory, ETH Zurich, Switzerland

<sup>2</sup> VISICS, ESAT/PSI, KU Leuven, Belgium

{nipopovic, paudel, probstt, vangool}@vision.ee.ethz.ch

In this supplementary document, we first give additional details on our implementation and experimental setup, which are contained in Section A. In Section B, we complement the results from the main paper by showing additional comparisons and studies regarding the training process, privacy preservation, adversarial robustness, confidence calibration, and transfer learning. We round off the document by a discussion of the effect and rationale of our design choices, as well as several aspects of our experimental findings, which can be found in Section C.

## A Additional implementation details

### A.1 Monte Carlo Inference

It has been demonstrated in the literature that the posterior distribution on the network weights  $w$  can be estimated using monte-carlo sampling in the context of dropout [27,45,26]. This way, predictions are integrated implicitly over the posterior distribution of the network weights  $q(w)$  as,

$$p(y|x) \approx \int p(y|x, w)q(w)dw \approx \frac{1}{T} \sum_{t=1}^T p(y|x, \hat{w}_t), \quad (1)$$

approximated by  $T$  samples  $\hat{w}_t$  [26], generated by applying dropout during inference. The posterior distribution  $p(y|x)$  also contains information about model uncertainty. Since our stochastic layers naturally offer such sampling for vision transformers, our goal is to investigate their effect on network calibration, as well as other applications, when performing inference with (1).

### A.2 Expectation over Transformation (EoT) Adversarial Attack

When dealing with stochasticity inside the network, Athalye et al. [2] demonstrated that for the class of randomness-based defenses, an expectation-over-transformation (EOT) attack is more effective, because of common gradient obfuscation. This can be viewed as using PGD [62] with the proxy gradient,

$$\mathbb{E}_{q(w)} [\nabla_x \mathcal{L}(f(\hat{x}^{k-1}, w), l)] \approx \frac{1}{T} \sum_{t=1}^T \nabla_x \mathcal{L}(f(\hat{x}^{k-1}, w_t), l), \quad (2)$$

where  $q(w)$  represents the distribution of the noise  $w \sim q(w)$  injected into the randomized classifier  $f(x, w)$ .

### A.3 Training our stochastic layers

When fine-tuning our network to adapt to the stochastic layers with  $a^j \sim \mathcal{U}(1 - \Delta, 1 + \Delta)$  (from Equation (8) of the main paper), we gradually adjust  $\Delta$  from 0 to its final value during the first third of the training epochs. When we use Dropout as a baseline, while matching the variance of  $a^j \sim \mathcal{U}(1 - \Delta, 1 + \Delta)$ , we also increase the drop probability from 0 to its final value in this manner. The same goes for the baseline which independently draws  $a^j \sim \mathcal{U}(1 - \Delta, 1 + \Delta)$  for each token – non-token-consistent. Also, in the experiment with adversarial training (see Section 5.3 of the main paper) and in experiments when we train from scratch (see Table 1c of the main paper), we use the same  $\Delta$  scheduling rule.

### A.4 Collaborative inference

When performing the experiments mentioned in Figure 4 of the main paper, we train the reconstruction decoder for 100 epochs with a batch size of 32. The weights of the client network  $\Phi_1(x)$ , which produces the feature maps, are frozen. The stochasticity remains turned on during both training and testing.

### A.5 Collaborative learning

When performing the experiments mentioned in Figure 5 of the main paper, the client network  $\Phi_1(x)$  is the part of the transformer which produces the feature map and its weights are frozen. The server network  $\Phi_2(x)$  is a small classifier with 2 fully connected layers, followed by a softmax.  $\Phi_2(x)$  is trained for a 100 epochs, with the learning rate of 0.0001 and the AdamW optimizer. The learning rate is divided by 10 after 50 epochs. The stochasticity remains turned on during both training and inference.

## B Further analysis

In this section, we perform a further analysis of the experiments presented in Section 5 of the main paper.

Table 1 is an extended version of Table 1a of the main paper. We see that there is no significant drop in accuracy when using our stochastic layers. To a brief discussion on the slightly better performance of regular dropout and non-token-consistent stochastic layers, please look at Section C.1 of this supplementary material and Section 5.1 of the main paper.

Next, we further analyse the problem discussed in Section 5.3 of the main paper. In Table 2 we see that our token-consistent stochastic layers achieve some



Table 1. **ImageNet-1k classification accuracy.** There is no significant drop in accuracy when using our token-consistent stochastic layers.

		Accuracy↑		
		No noise	$N = 1$	$N = 50$
DeiT-S		79.61%	79.61%	79.61%
DeiT-S + token-consistent ( $\Delta = 0.05$ )		79.79%	79.71%	79.81%
DeiT-S + token-consistent ( $\Delta = 0.1$ )		79.83%	79.58%	79.86%
DeiT-S + token-consistent ( $\Delta = 0.25$ )		79.87%	79.28%	79.88%
Training $\Delta = 0.5$	DeiT-S + token-consistent	79.60%	77.43%	79.72%
	DeiT-S + non-token-consistent	79.63%	78.59%	79.81%
	DeiT-S + dropout	79.60%	78.54%	79.79%
DeiT-S + token-consistent ( $\Delta = 0.75$ )		78.93%	75.46%	78.83%
Training ( $\Delta = 1.0$ )	DeiT-S + token-consistent	77.96%	72.93%	77.75%
	DeiT-S + non-token-consistent	77.99%	75.85%	78.63%
	DeiT-S + dropout	77.93%	76.18%	78.74%

Table 2. **Adversarial robustness, without adversarial training.** We see that using token-consistent stochastic layers achieves some level of robustness without adversarial training. This is not the case for the regular transformer. We also observe that the EoT attack does not fully penetrate the stochastic defense in this case.

		Accuracy ↑ (Without adversarial training)				
		Clean samples	PDG-10 attack			
			$\epsilon = \frac{2}{255}$		$\epsilon = \frac{4}{255}$	
			EoT		EoT	
DeiT-S		<b>79.61%</b>	0.43%	0.43%	0.01%	0.01%
DeiT-S + ours ( $\Delta = 0.5$ )	$N = 1$	77.43%	5.25%	1.97%	1.41%	0.23%
	$N = 50$	79.72%	5.25%	1.85%	1.37%	0.23%
DeiT-S + ours ( $\Delta = 1.0$ )	$N = 1$	72.93%	12.7%	<b>4.80%</b>	4.77%	1.06%
	$N = 50$	77.75%	<b>12.36%</b>	4.77%	<b>4.76%</b>	<b>1.07%</b>

level of adversarial robustness without using adversarial training. This is not the case for the regular transformer.

In the following, we further analyse the problem of collaborative inference discussed in Section 5.4 of the main paper. In Figure 1 we see examples of image reconstruction from the feature map of block 7 of the transformer. The first row depicts the original image. The second row depicts images reconstructed from the feature map of a deterministic network. Finally, the third row depicts reconstructions from our stochastic network. In particular the facial details are more degraded by our stochastic layers.

Now, we further analyse the problem of collaborative learning discussed in Section 5.4 of the main paper. In Table 3 we observe the results of learning a classifier on CIFAR-10 with features before and after the activation function. We observe that using features before the activation function to learn a classifier achieves better performance than when using features after the activation. This justifies the choice of using the features before the ReLU activation, in collaborative learning experiments.

Finally, we further analyse the problem of transfer learning from Section 5.5 of the main paper. In Table 4 we observe that our token-consistent stochastic



Fig. 1. **Privacy preservation in collaborative inference.** Reconstructed images from block 7 of the transformer with and without our token-consistent stochastic layers. First row depicts the original image. The second row depicts images reconstructed from the feature map of a deterministic transformer. Finally, the third row depicts reconstructions from our stochastic network. Our token-consistent stochastic layers preserve more privacy, in particular in the facial details.

Table 3. **Learning a classifier on CIFAR-10 with features before and after the activation function.** Using features before the activation function to learn a classifier achieves better performance than when using features after the activation.

	Accuracy↑							
	$\Delta = 0$		$\Delta = 0.1$		$\Delta = 0.5$		$\Delta = 1.0$	
	Before activation	After activation	Before activation	After activation	Before activation	After activation	Before activation	After activation
Block 6	74.44%	75.93%	71.31%	74.54%	59.45%	62.79%	47.75%	49.09%
Block 8	90.51%	81.27%	90.04%	81.67%	85.64%	77.18%	76.11%	68.07%
Block 10	94.07%	87.48%	94.03%	86.99%	91.9%	84.37%	85.97%	77.90%
Block 12	93.54%	88.98%	93.44%	89.19%	91.27%	86.68%	86.06%	80.55%

layers are able to retain their transfer learning performance and sometimes even exceed the deterministic baseline.

In Figures 2a, 2b and 2c we see histograms of barcode distances [34,11] of feature maps before and after the stochasticity is injected. The feature maps are obtained from the last block of the transformer. Histograms are constructed from 1000 randomly chosen input images from the validation set. The stochasticity level is  $\Delta = 0.5$ . In Figures 2d, 2e and 2f we can see the barcode persistence diagrams for a randomly chosen input image for dropout, non-token-consistent and token-consistent stochastic layers, respectively. Based on small distances of our method before and after injecting stochasticity, we conclude that the topological structure of token features is preserved. For a brief discussion on this experiment, please see Section C.3.

In Figure 3 we see histograms of average barcode distances between 4 samples for our stochastic network and the deterministic baseline. Stochasticity with the level of  $\Delta = 0.5$  is turned on for both the stochastic network and the deterministic baseline as well. We take the feature map from the last block of the

Table 4. **Transfer learning.** Transformers with our token-consistent stochastic layers are able to retain their performance and sometimes even exceed the deterministic baseline.

Dataset	Regular pre-training	$\Delta$ during pre-training					
		0.5			1.0		
		Token-consistent	Non-token-consistent	Dropout	Token-consistent	Non-token-consistent	Dropout
Aircraft	72.34%	71.50%	73.18%	72.46%	72.40%	71.71%	70.15%
Birdsnap	70.41%	69.58%	70.64%	70.33%	70.00%	70.19%	69.80%
CIFAR-10	98.11%	98.13%	98.35%	98.16%	98.29%	98.35%	98.35%
CIFAR-100	87.41%	87.65%	87.68%	87.82%	88.04%	87.87%	87.54%
Caltech-101	91.89%	91.89%	91.78%	91.69%	91.85%	92.21%	92.83%
Caltech-256	83.85%	84.07%	83.85%	83.78%	83.99%	83.52%	83.06%
Cars	80.76%	81.52%	80.94%	81.54%	81.99%	82.34%	81.46%
DTD	73.46%	73.94%	74.31%	74.95%	73.94%	72.71%	73.19%
Flowers	92.39%	93.69%	93.58%	93.28%	93.61%	93.43%	92.52%
Food	87.06%	87.10%	87.12%	87.25%	87.29%	86.95%	87.05%
Pets	92.83%	93.16%	92.86%	92.89%	93.08%	92.89%	93.02%
SUN397	62.34%	62.79%	62.72%	62.29%	62.36%	62.41%	62.25%

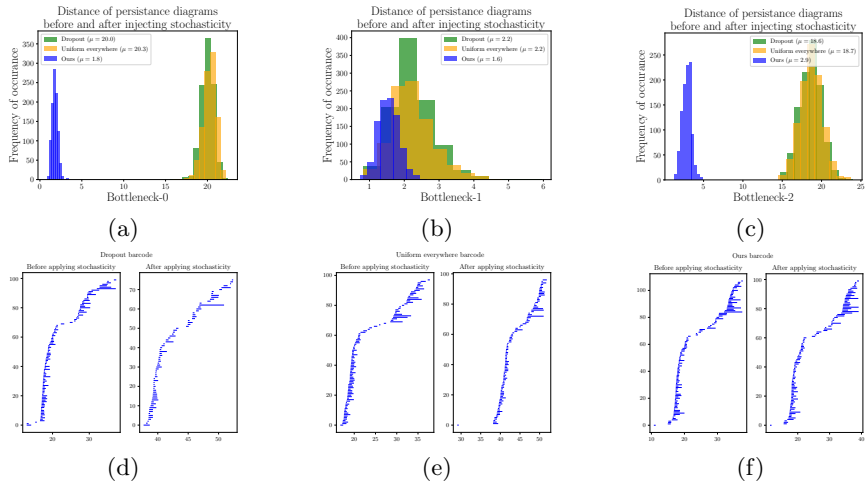
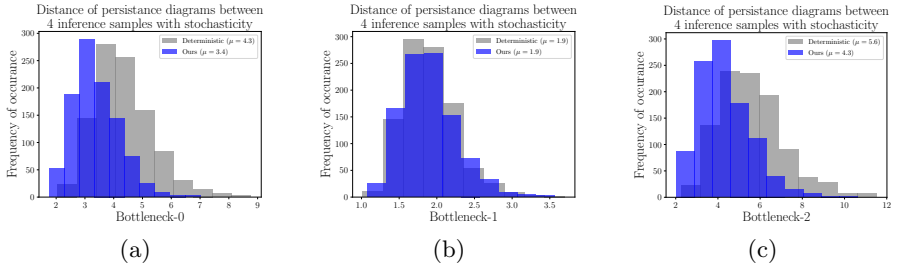


Fig. 2. **Persistence barcode diagrams before and after injecting stochasticity.** We analyze persistence barcode diagrams of feature maps before and after the stochasticity is injected. The histograms in Figures 2a, 2b and 2c correspond to barcode distances using simplex-0, simplex-1 and simplex-2, respectively. The feature maps are from the last block of the transformer. Histograms are constructed from 1000 randomly chosen input images from the validation set. The stochasticity level is  $\Delta = 0.5$ . In Figures 2d, 2e and 2f we can see the barcode persistence diagrams for a randomly chosen input image for dropout, non-token-consistent and token-consistent stochastic layers, respectively. Based on small distances of our method before and after injecting stochasticity, we conclude that the topological structure of token features is preserved, like it was mentioned in Section 3 of the main paper.



**Fig. 3. Distance of persistence barcode diagrams between 4 stochasticity samples for the same input.** We see histograms of average barcode distances between 4 stochasticity draws for the same input image. Stochasticity with the level of  $\Delta = 0.5$  is turned on for both the stochastic network and the deterministic baseline as well. The histograms in Figures 2a, 2b and 2c correspond to using simplex-0, simplex-1 and simplex-2, respectively. We take the feature map from the last block of the transformer, right before the stochasticity is injected, and sample 4 inference forward passes. Histograms are constructed from 1000 randomly chosen input images from the validation set. We observe that when a stochasticity is injected, feature maps of our stochastic network have a more consistent topology (lower barcode distances) compared to the deterministic baseline.

transformer, right before the stochasticity is injected, and sample 4 inference forward passes. Histograms are constructed from 1000 randomly chosen input images from the validation set. We observe that when a stochasticity is injected, feature maps of our stochastic network have a more consistent topology (lower barcode distances) compared to the deterministic baseline. For a brief discussion of this experiment, please see Section C.3.

## C Discussion

### C.1 Difference to standard Dropout

**Theoretical.** In its original formulation, dropout [89] aims to prevent co-adaptation of neurons through randomly dropping activations, thus creating randomized neural pathways in fully-connected layers. In the case of CNNs, 2D dropout (SpatialDropout) [91] has found to be a more effective regularization, due to the high correlation of nearby pixels. In the case of vision transformers [20] however, information of neighbouring pixels is collapsed into token features (pixels within the same input patch) as well as across tokens (pixels of different input patches). Therefore, the concept of neighbourhood gets ‘diluted’, and the conclusions of [89] and [91] are in a state of conflict when it comes to vision transformers. On the other hand, our token-consistent stochastic layers are designed for transformer-based architectures, and we draw our theoretical motivations from the homeomorphic nature of their operation – by applying the same noise on all tokens (see Section 3 of the main paper). Furthermore, to obtain stochastic

homeomorphisms, we avoid noise distributions that violate invertibility of the operation, in particular the Bernoulli noise employed by [89,91]. We therefore choose uniform noise in our experiments.

**Experimental.** In practice, we observe the different effects of our token-consistent stochastic layers and dropout in several settings. For instance, our token-consistent method offers better confidence calibration than dropout and the non-token consistent version, as shown in Table 2 of the main paper. This pattern coincides with several observations on other tasks. For example, in Figure 4 of the main paper, it can be observed that injecting stochasticity through non-homeomorphic operations, such as dropout and the non-token-consistent counterpart, preserves less privacy. Also, our token-consistent stochastic layers provide stronger stochasticity to the network under the same variance, even though the random variables are the same for each token. This can be observed on ImageNet-1k classification accuracy shown in Table 1. The non-homeomorphic operations dropout and the non-token-consistent baseline tend to retain more accuracy of the original network (e.g. with  $N = 1$  sample).

## C.2 Fine-tuning vs. training from scratch

Fine-tuning brings the benefit of being able to quickly integrate our stochastic layers into an already trained network. In this process, the architecture of the original transformer is unchanged, while at the same time we can enjoy the benefits discussed in Section 5 of the main paper. This saves a lot of training cost and  $CO_2$  emissions. This does not significantly degrade ImageNet-1k classification accuracy as can be seen in Figure 3 of the main paper. Moreover, we demonstrated that training the network from scratch with our stochastic layers is possible, even with strong stochasticity, in Table 1c in the main paper.

## C.3 Topology

In Figure 2 we show histograms of barcode distances of feature maps before and after the stochasticity is injected. Based on small topological distances of features before and after injecting stochasticity with our token-consistent stochastic layers, we conclude that the topological structure of token features is preserved. This experiment complements the theory of Section 3 in the main paper.

In Figure 3 we see histograms of average barcode distances between 4 stochastic samples for the same input image for our stochastic layers and the deterministic baseline. We observe that feature maps of our stochastic network have a more consistent topology (lower barcode distances) compared to the deterministic baseline, when stochasticity is injected. Even though the deterministic baseline is not trained with the stochasticity, the stochasticity injected during inference preserves the topological structure of the feature map. Nevertheless, following layers damage that topological structure. However, when the network is trained with this stochasticity source which preserves the feature map topology, following layers do less damage to the topological structure.

## C.4 Regularization effect

It is known that stochasticity can have a regularizing effect [89]. In fact, our results in Table 1c of the main paper hint in this direction when training from scratch. However, we did not further investigate this behaviour due to the reasons discussed in Section C.2 and also because it is not the main focus of this paper.

## C.5 Ethical and Societal Impact.

This work is concerned with the learning of improved visual features by noise injection. Even though these features offer better resilience on privacy and adversarial attacks, they do not meet a certifiable standard as of now. Therefore they should not be used in a production system without additional layers of safety measures, such as encryption or humans-in-the-loop. Although our method allows for an improved estimation of prediction confidence overall, we did not investigate the behaviour with regards to specific subgroups of classes or people. This needs to be carefully analysed with appropriate datasets to mitigate discriminatory actions by a decision-making system based on our algorithm.

## References

1. Alemi, A.A., Fischer, I.S., Dillon, J.V., Murphy, K.P.: Deep variational information bottleneck. ArXiv [abs/1612.00410](https://arxiv.org/abs/1612.00410) (2017)
2. Athalye, A., Carlini, N., Wagner, D.A.: Obfuscated gradients give a false sense of security: Circumventing defenses to adversarial examples. In: ICML (2018)
3. Athalye, A., Engstrom, L., Ilyas, A., Kwok, K.: Synthesizing robust adversarial examples. ArXiv [abs/1707.07397](https://arxiv.org/abs/1707.07397) (2018)
4. Ba, J.L., Kiros, J.R., Hinton, G.E.: Layer normalization (2016)
5. Basu, S., Izmailov, R., Mesterharm, C.: Membership model inversion attacks for deep networks. ArXiv [abs/1910.04257](https://arxiv.org/abs/1910.04257) (2019)
6. Berg, T., Liu, J., Lee, S.W., Alexander, M.L., Jacobs, D.W., Belhumeur, P.N.: Birdsnap: Large-scale fine-grained visual categorization of birds. 2014 IEEE Conference on Computer Vision and Pattern Recognition pp. 2019–2026 (2014)
7. Bonawitz, K., Eichner, H., Grieskamp, W., Huba, D., Ingerman, A., Ivanov, V., Kiddon, C., Konečný, J., Mazzocchi, S., McMahan, H.B., et al.: Towards federated learning at scale: System design. arXiv preprint [arXiv:1902.01046](https://arxiv.org/abs/1902.01046) (2019)
8. Bossard, L., Guillaumin, M., Gool, L.V.: Food-101 - mining discriminative components with random forests. In: ECCV (2014)
9. Buckman, J., Roy, A., Raffel, C., Goodfellow, I.: Thermometer encoding: One hot way to resist adversarial examples (2018), <https://openreview.net/pdf?id=S18Su--CW>
10. Carion, N., Massa, F., Synnaeve, G., Usunier, N., Kirillov, A., Zagoruyko, S.: End-to-end object detection with transformers. In: ECCV. pp. 213–229. Springer (2020)
11. Chazal, F., Michel, B.: An introduction to topological data analysis: fundamental and practical aspects for data scientists. *Frontiers in Artificial Intelligence* **4** (2021)

12. Cimpoi, M., Maji, S., Kokkinos, I., Mohamed, S., Vedaldi, A.: Describing textures in the wild. 2014 IEEE Conference on Computer Vision and Pattern Recognition pp. 3606–3613 (2014)
13. Cissé, M., Bojanowski, P., Grave, E., Dauphin, Y., Usunier, N.: Parseval networks: Improving robustness to adversarial examples. ArXiv [abs/1704.08847](#) (2017)
14. Cohen, J.M., Rosenfeld, E., Kolter, J.Z.: Certified adversarial robustness via randomized smoothing. In: ICML (2019)
15. Croce, F., Andriushchenko, M., Hein, M.: Provable robustness of relu networks via maximization of linear regions. ArXiv [abs/1810.07481](#) (2019)
16. Cubuk, E.D., Zoph, B., Shlens, J., Le, Q.V.: Randaugment: Practical automated data augmentation with a reduced search space. 2020 IEEE/CVF Conference on Computer Vision and Pattern Recognition Workshops (CVPRW) pp. 3008–3017 (2020)
17. Dai, B., Zhu, C., Wipf, D.P.: Compressing neural networks using the variational information bottleneck. ArXiv [abs/1802.10399](#) (2018)
18. Dai, Z., Yang, Z., Yang, Y., Carbonell, J., Le, Q.V., Salakhutdinov, R.: Transformer-XL: Attentive language models beyond a fixed-length context. In: Annual Meeting of the Association for Computational Linguistics (ACL). pp. 2978–2988 (2019)
19. Devlin, J., Chang, M.W., Lee, K., Toutanova, K.: BERT: Pre-training of deep bidirectional transformers for language understanding. In: NAACL-HLT. pp. 4171–4186 (2019)
20. Dosovitskiy, A., Beyer, L., Kolesnikov, A., Weissenborn, D., Zhai, X., Unterthiner, T., Dehghani, M., Minderer, M., Heigold, G., Gelly, S., Uszkoreit, J., Houlsby, N.: An image is worth 16x16 words: Transformers for image recognition at scale. In: ICLR (2021)
21. Durasov, N., Bagautdinov, T., Baque, P., Fua, P.: Masksembles for Uncertainty Estimation (2021)
22. Engelsma, J.J., Jain, A.K., Boddeti, V.N.: Hers: Homomorphically encrypted representation search. ArXiv [abs/2003.12197](#) (2020)
23. Fang, H.S.A., Qian, Q.: Privacy preserving machine learning with homomorphic encryption and federated learning. *Future Internet* **13**, 94 (2021)
24. Fei-Fei, L., Fergus, R., Perona, P.: Learning generative visual models from few training examples: An incremental bayesian approach tested on 101 object categories. In: CVPR Workshops (2004)
25. Finlay, C., Oberman, A.M.: Scaleable input gradient regularization for adversarial robustness. ArXiv [abs/1905.11468](#) (2019)
26. Gal, Y., Ghahramani, Z.: Bayesian convolutional neural networks with bernoulli approximate variational inference. ArXiv [abs/1506.02158](#) (2015)
27. Gal, Y., Ghahramani, Z.: Dropout as a bayesian approximation: Representing model uncertainty in deep learning. ArXiv [abs/1506.02142](#) (2016)
28. Geppert, M., Larsson, V., Speciale, P., Schönberger, J.L., Pollefeys, M.: Privacy preserving structure-from-motion. In: ECCV (2020)
29. Goodfellow, I.J., Shlens, J., Szegedy, C.: Explaining and harnessing adversarial examples. CoRR [abs/1412.6572](#) (2015)
30. Griffin, G., Holub, A., Perona, P.: Caltech-256 object category dataset (2007)
31. Gu, S.S., Rigazio, L.: Towards deep neural network architectures robust to adversarial examples. CoRR [abs/1412.5068](#) (2015)
32. Guo, C., Pleiss, G., Sun, Y., Weinberger, K.Q.: On calibration of modern neural networks. In: International Conference on Machine Learning. pp. 1321–1330. PMLR (2017)

33. Gupta, O., Raskar, R.: Distributed learning of deep neural network over multiple agents. *Journal of Network and Computer Applications* **116**, 1–8 (2018)
34. Guss, W.H., Salakhutdinov, R.: On characterizing the capacity of neural networks using algebraic topology. arXiv preprint arXiv:1802.04443 (2018)
35. He, K., Zhang, X., Ren, S., Sun, J.: Deep residual learning for image recognition. arXiv preprint arXiv:1512.03385 (2015)
36. Hsu, C.Y., Lu, C.S., Pei, S.C.: Image feature extraction in encrypted domain with privacy-preserving sift. *IEEE Transactions on Image Processing* **21**, 4593–4607 (2012)
37. Huang, G., Sun, Y., Liu, Z., Sedra, D., Weinberger, K.: Deep networks with stochastic depth (2016)
38. Ilyas, A., Santurkar, S., Tsipras, D., Engstrom, L., Tran, B., Madry, A.: Adversarial examples are not bugs, they are features. ArXiv **abs/1905.02175** (2019)
39. Isola, P., Zhu, J.Y., Zhou, T., Efros, A.A.: Image-to-image translation with conditional adversarial networks (2018)
40. Izmailov, P., Podoprikin, D., Garipov, T., Vetrov, D., Wilson, A.G.: Averaging weights leads to wider optima and better generalization. arXiv preprint arXiv:1803.05407 (2018)
41. Jakubovitz, D., Giryas, R.: Improving dnn robustness to adversarial attacks using jacobian regularization. ArXiv **abs/1803.08680** (2018)
42. Kairouz, P., McMahan, H.B., Avent, B., Bellet, A., Bennis, M., Bhagoji, A.N., Bonawitz, K., Charles, Z., Cormode, G., Cummings, R., et al.: Advances and open problems in federated learning. arXiv preprint arXiv:1912.04977 (2019)
43. Karras, T., Laine, S., Aila, T.: A style-based generator architecture for generative adversarial networks. 2019 IEEE/CVF Conference on Computer Vision and Pattern Recognition (CVPR) pp. 4396–4405 (2019)
44. Kaur, S., Cohen, J.M., Lipton, Z.C.: Are perceptually-aligned gradients a general property of robust classifiers? CoRR **abs/1910.08640** (2019), <http://arxiv.org/abs/1910.08640>
45. Kendall, A., Gal, Y.: What uncertainties do we need in bayesian deep learning for computer vision? In: NIPS (2017)
46. Khan, S., Naseer, M., Hayat, M., Zamir, S.W., Khan, F.S., Shah, M.: Transformers in vision: A survey. arXiv preprint arXiv:2101.01169 (2021)
47. Kingma, D.P., Salimans, T., Welling, M.: Variational dropout and the local reparameterization trick. ArXiv **abs/1506.02557** (2015)
48. Kingma, D.P., Welling, M.: Auto-encoding variational bayes. CoRR **abs/1312.6114** (2014)
49. Konecný, J., McMahan, H.B., Yu, F.X., Richtárik, P., Suresh, A.T., Bacon, D.: Federated learning: Strategies for improving communication efficiency. ArXiv **abs/1610.05492** (2016)
50. Kornblith, S., Shlens, J., Le, Q.V.: Do better imagenet models transfer better? 2019 IEEE/CVF Conference on Computer Vision and Pattern Recognition (CVPR) pp. 2656–2666 (2019)
51. Krause, J., Deng, J., Stark, M., Fei-Fei, L.: Collecting a large-scale dataset of fine-grained cars (2013)
52. Krizhevsky, A.: Learning multiple layers of features from tiny images (2009)
53. Kurakin, A., Goodfellow, I.J., Bengio, S.: Adversarial examples in the physical world. CoRR **abs/1607.02533** (2016), <http://arxiv.org/abs/1607.02533>
54. Kurakin, A., Goodfellow, I.J., Bengio, S.: Adversarial machine learning at scale. ArXiv **abs/1611.01236** (2017)



55. Lakshminarayanan, B., Pritzel, A., Blundell, C.: Simple and scalable predictive uncertainty estimation using deep ensembles (2017)
56. Laves, M.H., Ihler, S., Kortmann, K.P., Ortmaier, T.: Calibration of model uncertainty for dropout variational inference. ArXiv [abs/2006.11584](https://arxiv.org/abs/2006.11584) (2020)
57. Lee, S., Kim, H., Lee, J.: Graddiv: Adversarial robustness of randomized neural networks via gradient diversity regularization. ArXiv [abs/2107.02425](https://arxiv.org/abs/2107.02425) (2021)
58. Li, A., Guo, J., Yang, H., Salim, F.D., Chen, Y.: Deepobfuscator: Obfuscating intermediate representations with privacy-preserving adversarial learning on smartphones. In: Proceedings of the International Conference on Internet-of-Things Design and Implementation. p. 28–39. IoTDI '21, Association for Computing Machinery, New York, NY, USA (2021). <https://doi.org/10.1145/3450268.3453519>, <https://doi.org/10.1145/3450268.3453519>
59. LingChen, T.C., Khonsari, A., Lashkari, A., Nazari, M.R., Sambee, J.S., Nascimento, M.A.: Uniformaugmt: A search-free probabilistic data augmentation approach. ArXiv [abs/2003.14348](https://arxiv.org/abs/2003.14348) (2020)
60. Liu, Z., Lin, Y., Cao, Y., Hu, H., Wei, Y., Zhang, Z., Lin, S., Guo, B.: Swin transformer: Hierarchical vision transformer using shifted windows (2021)
61. Loshchilov, I., Hutter, F.: Fixing weight decay regularization in adam. CoRR [abs/1711.05101](https://arxiv.org/abs/1711.05101) (2017), <http://arxiv.org/abs/1711.05101>
62. Madry, A., Makelov, A., Schmidt, L., Tsipras, D., Vladu, A.: Towards deep learning models resistant to adversarial attacks. ArXiv [abs/1706.06083](https://arxiv.org/abs/1706.06083) (2018)
63. Maji, S., Kannala, J., Rahtu, E., Blaschko, M., Vedaldi, A.: Fine-grained visual classification of aircraft. Tech. rep. (2013)
64. Mihajlović, M., Popović, N.: Fooling a neural network with common adversarial noise. In: 2018 19th IEEE Mediterranean Electrotechnical Conference (MELECON). pp. 293–296 (2018). <https://doi.org/10.1109/MELCON.2018.8379110>
65. Minderer, M., Djolonga, J., Romijnders, R., Hubis, F.A., Zhai, X., Houlsby, N., Tran, D., Lucic, M.: Revisiting the calibration of modern neural networks. ArXiv [abs/2106.07998](https://arxiv.org/abs/2106.07998) (2021)
66. Mordido, G., Yang, H., Meinel, C.: Dropout-gan: Learning from a dynamic ensemble of discriminators. ArXiv [abs/1807.11346](https://arxiv.org/abs/1807.11346) (2018)
67. Naeini, M.P., Cooper, G.F., Hauskrecht, M.: Obtaining well calibrated probabilities using bayesian binning. Proceedings of the ... AAAI Conference on Artificial Intelligence. AAAI Conference on Artificial Intelligence **2015**, 2901–2907 (2015)
68. Neelakantan, A., Vilnis, L., Le, Q.V., Sutskever, I., Kaiser, L., Kurach, K., Martens, J.: Adding gradient noise improves learning for very deep networks. ArXiv [abs/1511.06807](https://arxiv.org/abs/1511.06807) (2015)
69. Niculescu-Mizil, A., Caruana, R.: Predicting good probabilities with supervised learning. In: Proceedings of the 22nd International Conference on Machine Learning. p. 625–632. ICML '05, Association for Computing Machinery, New York, NY, USA (2005). <https://doi.org/10.1145/1102351.1102430>, <https://doi.org/10.1145/1102351.1102430>
70. Nilsback, M.E., Zisserman, A.: Automated flower classification over a large number of classes. 2008 Sixth Indian Conference on Computer Vision, Graphics & Image Processing pp. 722–729 (2008)
71. Ororbia, A., Giles, C.L., Kifer, D.: Unifying adversarial training algorithms with flexible deep data gradient regularization. ArXiv [abs/1601.07213](https://arxiv.org/abs/1601.07213) (2016)
72. Panousis, K., Chatzis, S., Alexos, A., Theodoridis, S.: Local competition and stochasticity for adversarial robustness in deep learning. In: International Conference on Artificial Intelligence and Statistics. pp. 3862–3870. PMLR (2021)

73. Parkhi, O.M., Vedaldi, A., Zisserman, A., Jawahar, C.V.: Cats and dogs. 2012 IEEE Conference on Computer Vision and Pattern Recognition pp. 3498–3505 (2012)
74. Pinot, R., Meunier, L., Araujo, A., Kashima, H., Yger, F., Gouy-Pailler, C., Atif, J.: Theoretical evidence for adversarial robustness through randomization. In: NeurIPS (2019)
75. Pittaluga, F., Koppal, S.J., Kang, S.B., Sinha, S.N.: Revealing scenes by inverting structure from motion reconstructions. 2019 IEEE/CVF Conference on Computer Vision and Pattern Recognition (CVPR) pp. 145–154 (2019)
76. Qin, Z., Yan, J., Ren, K., Chen, C.W., Wang, C.: Towards efficient privacy-preserving image feature extraction in cloud computing. Proceedings of the 22nd ACM international conference on Multimedia (2014)
77. Rakin, A.S., He, Z., Fan, D.: Parametric noise injection: Trainable randomness to improve deep neural network robustness against adversarial attack. 2019 IEEE/CVF Conference on Computer Vision and Pattern Recognition (CVPR) pp. 588–597 (2019)
78. Ross, A.S., Doshi-Velez, F.: Improving the adversarial robustness and interpretability of deep neural networks by regularizing their input gradients. In: AAAI (2018)
79. Roy, P.C., Boddeti, V.N.: Mitigating information leakage in image representations: A maximum entropy approach. 2019 IEEE/CVF Conference on Computer Vision and Pattern Recognition (CVPR) pp. 2581–2589 (2019)
80. Russakovsky, O., Deng, J., Su, H., Krause, J., Satheesh, S., Ma, S., Huang, Z., Karpathy, A., Khosla, A., Bernstein, M., Berg, A.C., Fei-Fei, L.: ImageNet Large Scale Visual Recognition Challenge. International Journal of Computer Vision (IJCV) **115**(3), 211–252 (2015). <https://doi.org/10.1007/s11263-015-0816-y>
81. Salman, H., Ilyas, A., Engstrom, L., Kapoor, A., Madry, A.: Do adversarially robust imagenet models transfer better? (2020)
82. Salman, H., Yang, G., Li, J., Zhang, P., Zhang, H., Razenshteyn, I.P., Bubeck, S.: Provably robust deep learning via adversarially trained smoothed classifiers. In: NeurIPS (2019)
83. Shafahi, A., Najibi, M., Ghiasi, A., Xu, Z., Dickerson, J.P., Studer, C., Davis, L.S., Taylor, G., Goldstein, T.: Adversarial training for free! In: NeurIPS (2019)
84. Shridhar, K., Laumann, F., Liwicki, M.: A comprehensive guide to bayesian convolutional neural network with variational inference. arXiv preprint arXiv:1901.02731 (2019)
85. Singh, A., Chopra, A., Sharma, V., Garza, E., Zhang, E., Vepakomma, P., Raskar, R.: Disco: Dynamic and invariant sensitive channel obfuscation for deep neural networks. 2021 IEEE/CVF Conference on Computer Vision and Pattern Recognition (CVPR) pp. 12120–12130 (2021)
86. Smith, S.L., Dherin, B.R.U., Barrett, D.G.T., De, S.: On the origin of implicit regularization in stochastic gradient descent. ArXiv **abs/2101.12176** (2021)
87. Spall, J.C.: Introduction to stochastic search and optimization: estimation, simulation, and control, vol. 65. John Wiley & Sons (2005)
88. Speciale, P., Schönberger, J.L., Kang, S.B., Sinha, S.N., Pollefeys, M.: Privacy preserving image-based localization. 2019 IEEE/CVF Conference on Computer Vision and Pattern Recognition (CVPR) pp. 5488–5498 (2019)
89. Srivastava, N., Hinton, G., Krizhevsky, A., Sutskever, I., Salakhutdinov, R.: Dropout: a simple way to prevent neural networks from overfitting. The journal of machine learning research **15**(1), 1929–1958 (2014)

90. Szegedy, C., Zaremba, W., Sutskever, I., Bruna, J., Erhan, D., Goodfellow, I.J., Fergus, R.: Intriguing properties of neural networks. CoRR **abs/1312.6199** (2014)
91. Tompson, J., Goroshin, R., Jain, A., LeCun, Y., Bregler, C.: Efficient object localization using convolutional networks. 2015 IEEE Conference on Computer Vision and Pattern Recognition (CVPR) pp. 648–656 (2015)
92. Touvron, H., Cord, M., Douze, M., Massa, F., Sablayrolles, A., Jegou, H.: Training data-efficient image transformers & distillation through attention. In: International Conference on Machine Learning. vol. 139, pp. 10347–10357 (July 2021)
93. Ulyanov, D., Vedaldi, A., Lempitsky, V.S.: Deep image prior. 2018 IEEE/CVF Conference on Computer Vision and Pattern Recognition pp. 9446–9454 (2018)
94. Vaswani, A., Shazeer, N., Parmar, N., Uszkoreit, J., Jones, L., Gomez, A.N., Kaiser, L.u., Polosukhin, I.: Attention is all you need. In: Guyon, I., Luxburg, U.V., Bengio, S., Wallach, H., Fergus, R., Vishwanathan, S., Garnett, R. (eds.) *Advances in Neural Information Processing Systems*. vol. 30. Curran Associates, Inc. (2017), <https://proceedings.neurips.cc/paper/2017/file/3f5ee243547dee91fbd053c1c4a845aa-Paper.pdf>
95. Vepakomma, P., Gupta, O., Swedish, T., Raskar, R.: Split learning for health: Distributed deep learning without sharing raw patient data. arXiv preprint arXiv:1812.00564 (2018)
96. Wang, P., Li, Y., Singh, K.K., Lu, J., Vasconcelos, N.: Imagine: Image synthesis by image-guided model inversion. 2021 IEEE/CVF Conference on Computer Vision and Pattern Recognition (CVPR) pp. 3680–3689 (2021)
97. Wang, W., Xie, E., Li, X., Fan, D.P., Song, K., Liang, D., Lu, T., Luo, P., Shao, L.: Pyramid vision transformer: A versatile backbone for dense prediction without convolutions. arXiv preprint arXiv:2102.12122 (2021)
98. Wang, Y., Xu, Z., Wang, X., Shen, C., Cheng, B., Shen, H., Xia, H.: End-to-end video instance segmentation with transformers. In: CVPR (2021)
99. Wong, E., Rice, L., Kolter, J.Z.: Fast is better than free: Revisiting adversarial training. ArXiv **abs/2001.03994** (2020)
100. xiong Xiao, J., Hays, J., Ehinger, K.A., Oliva, A., Torralba, A.: Sun database: Large-scale scene recognition from abbey to zoo. 2010 IEEE Computer Society Conference on Computer Vision and Pattern Recognition pp. 3485–3492 (2010)
101. Yang, Z., Dai, Z., Yang, Y., Carbonell, J., Salakhutdinov, R., Le, Q.V.: XLNet: Generalized autoregressive pretraining for language understanding. In: NIPS. pp. 5753–5763 (2019)
102. Yin, H., Molchanov, P., Li, Z., Álvarez, J.M., Mallya, A., Hoiem, D., Jha, N.K., Kautz, J.: Dreaming to distill: Data-free knowledge transfer via deepinversion. 2020 IEEE/CVF Conference on Computer Vision and Pattern Recognition (CVPR) pp. 8712–8721 (2020)
103. Yu, T., Yang, Y., Li, D., Hospedales, T., Xiang, T.: Simple and effective stochastic neural networks (2019)
104. Yuan, L., Chen, Y., Wang, T., Yu, W., Shi, Y., Tay, F.E., Feng, J., Yan, S.: Tokens-to-token ViT: Training vision transformers from scratch on imagenet. arXiv preprint arXiv:2101.11986 (2021)
105. Zhai, R., Dan, C., He, D., Zhang, H., Gong, B., Ravikumar, P., Hsieh, C.J., Wang, L.: Macer: Attack-free and scalable robust training via maximizing certified radius. ArXiv **abs/2001.02378** (2020)
106. Zhang, H.R., Yu, Y., Jiao, J., Xing, E.P., Ghaoui, L.E., Jordan, M.I.: Theoretically principled trade-off between robustness and accuracy. In: ICML (2019)

107. Zhang, Y., Jia, R., Pei, H., Wang, W., Li, B., Song, D.X.: The secret revealer: Generative model-inversion attacks against deep neural networks. 2020 IEEE/CVF Conference on Computer Vision and Pattern Recognition (CVPR) pp. 250–258 (2020)
108. Zheng, S., Lu, J., Zhao, H., Zhu, X., Luo, Z., Wang, Y., Fu, Y., Feng, J., Xiang, T., Torr, P.H., Zhang, L.: Rethinking semantic segmentation from a sequence-to-sequence perspective with transformers. In: CVPR (2021)